JB
Journals.ASM.org

# High Hydrostatic Pressure Induces Counterclockwise to Clockwise Reversals of the *Escherichia coli* Flagellar Motor

**Masayoshi Nishiyama,[a,b,c,d] Yoshiyuki Sowa,[e] Yoshifumi Kimura,[d,f] Michio Homma,[g] Akihiko Ishijima,[h] Masahide Terazima[d]**

The Hakubi Center for Advanced Research, Kyoto University, Kyoto, Japan[a]; Institute for Integrated Cell-Material Sciences, Kyoto University, Kyoto, Japan[b]; JST, PRESTO, Honcho Kawaguchi, Saitama, Japan[c]; Department of Chemistry, Kyoto University, Kyoto, Japan[d]; Department of Frontier Bioscience, Hosei University, Tokyo, Japan[e]; Department of Chemical Science and Technology, Hosei University, Tokyo, Japan[f]; Division of Biological Science, Nagoya University, Nagoya, Aichi, Japan[g]; Institute of Multidisciplinary Research for Advanced Materials, Tohoku University, Sendai, Japan[h]

**The bacterial flagellar motor is a reversible rotary machine that rotates a left-handed helical filament, allowing bacteria to swim toward a more favorable environment. The direction of rotation reverses from counterclockwise (CCW) to clockwise (CW), and vice versa, in response to input from the chemotaxis signaling circuit. CW rotation is normally caused by binding of the phosphorylated response regulator CheY (CheY-P), and strains lacking CheY are typically locked in CCW rotation. The detailed mechanism of switching remains unresolved because it is technically difficult to regulate the level of CheY-P within the concentration range that produces flagellar reversals. Here, we demonstrate that high hydrostatic pressure can induce CW rotation even in the absence of CheY-P. The rotation of single flagellar motors in *Escherichia coli* cells with the *cheY* gene deleted was monitored at various pressures and temperatures. Application of >120 MPa pressure induced a reversal from CCW to CW at 20°C, although at that temperature, no motor rotated CW at ambient pressure (0.1 MPa). At lower temperatures, pressure-induced changes in direction were observed at pressures of <120 MPa. CW rotation increased with pressure in a sigmoidal fashion, as it does in response to increasing concentrations of CheY-P. Application of pressure generally promotes the formation of clusters of ordered water molecules on the surfaces of proteins. It is possible that hydration of the switch complex at high pressure induces structural changes similar to those caused by the binding of CheY-P.**

*Escherichia coli* cells can sense and respond to many environmental factors, such as chemicals, pH, and temperature, and swim toward more favorable environments for them by rotating their helical flagella (1–5). Each flagellum includes a long (~10-μm), thin (~20-nm), helical filament that turns about its long axis either counterclockwise (CCW) (viewed from filament to motor) or clockwise (CW). CCW rotation allows the multiple filaments of a cell to form a helical bundle that propels the cell body smoothly in what is called a "run." A CW-rotating filament leaves the bundle and leads to a change in the swimming direction, called a "tumble." Regulating switching between CCW and CW rotation leads *E. coli* cells to bias a three-dimensional random walk to directional movements in liquid environments.

The bacterial flagellar motor converts the chemical energy of ion flux across the cell membrane to the rotation of a flagellum (6–10). The motor consists of a rotor and multiple stator units, and its major components are located in the cell membrane. The rotor spins relative to the cell body, and it is firmly connected to the flagellar filament, whereas the stator units are anchored to the cell wall. Torque is generated by intermolecular interactions between a rotor and stator units. The rotational direction is controlled by the binding of the phosphorylated form of the response regulator CheY (CheY-P) onto the rotor. The direction of flagellar rotation is highly dependent on the CheY-P concentration in a cell and is characterized by a Hill coefficient of ≈10 (11). This ultrasensitive switching is thought to be triggered by dynamic conformational changes in the switch complex of the rotor (12–15), but the detailed molecular mechanism of switching remains unresolved. This is because it is technically difficult to regulate the binding of CheY-P to the switch complex and to detect the resulting conformational changes under *in vivo* conditions.

Here, we show that applying high pressure modulates the rotational direction of bacterial flagellar motors *in vivo*. Hydrostatic pressure is one of the physical stimuli that characterize the environment of microorganisms (16, 17), and the pressure-induced changes could be visualized by high-pressure microscopy (18–22). *E. coli* is a representative research target for studying the mechanism by which hydrostatic pressure affects bacterial physiology, such as transmembrane transport (23, 24), protein and nucleic acid synthesis (25), enzymatic function (26), cell division (22, 27, 28), and growth (27–29). Most of these biogenic reactions are inhibited at less than 100 MPa. Hydrostatic pressure in the deepest part of the Mariana Trench (10,900 m in depth) is ~110 MPa. Flagellar motility has also been known to be sensitive to applied pressures (30, 31). We recently constructed a high-resolution, high-pressure microscope, and it appeared that application of 80 MPa of pressure inhibited the motility of smoothly swimming RP4979 cells (32, 33). Although the rotational speed of their flagellar motors gradually decreased with increased pressure, the motors rotated smoothly in the CCW direction even at 80 MPa, regardless of the viscous load.

In this study, we examined the effects of pressure on the motor rotation itself. The rotation of single flagellar motors in *E. coli* cells with the *cheY* gene deleted was monitored at various pressures and

**Received** 19 November 2012 **Accepted** 6 February 2013
**Published ahead of print** 15 February 2013
Address correspondence to Masayoshi Nishiyama, mnishiyama@icems.kyoto-u.ac.jp.
Supplemental material for this article may be found at http://dx.doi.org/10.1128/JB.02139-12.

doi:10.1128/JB.02139-12

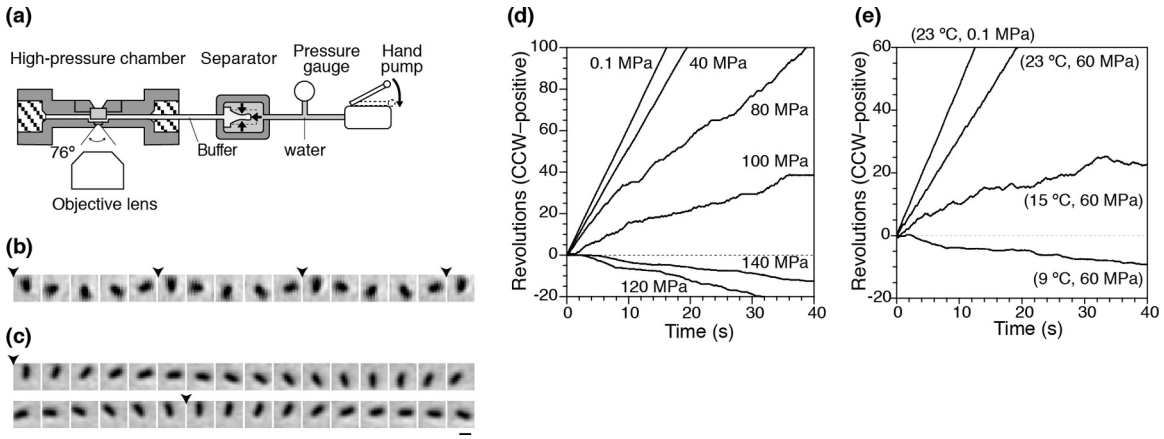


**FIG 1** Rotation of flagellar motors at high pressure. (a) High-pressure microscopy device (not to scale). (b and c) Sequential phase-contrast images of the same tethered cell at 33-ms intervals. The pressures were 0.1 (b) and 120 (c) MPa. The arrowheads indicate completion of a turn. Bar, 2 μm. (d and e) Time courses of rotations of individual cells (CCW positive). (d) The experimental temperature was 20°C, and the pressure was increased from 0.1 to 140 MPa. (e) Pressure was held at 60 MPa, and the temperature was decreased from 23 to 9°C.

temperatures. We found that application of >120 MPa pressure induced a reversal from CCW to CW rotation at 20°C, although at that temperature, no motor rotated CW at ambient pressure (0.1 MPa). At lower temperatures, pressure-induced changes in direction were observed at pressures of <120 MPa. Our results indicated that increased pressure and decreased temperature act in a complementary fashion to reverse motor rotation from CCW to CW. This is consistent with a previous study in which flagellar motors rotated exclusively CW at −2°C and 0.1 MPa (34). CW rotation increased with pressure in a sigmoidal fashion, as it does in response to increasing concentrations of CheY-P. The results reported provide insight into the structural changes that may be involved in CheY-mediated reversals of the rotational direction of bacterial flagellar motors.

## MATERIALS AND METHODS

**Bacterial strain.** We used *E. coli* strain YS1217 (32), which was constructed from strain JHC36 (*fliC-sticky* Δ*cheY* Δ*motA* Δ*motB*) (35) by transformation with plasmid pDFB27 (*motA motB*, arabinose inducible; Ap$^r$) (36). The flagellar-filament protein with amino acids 245 to 301 deleted is encoded by *fliC-sticky* in the chromosome and adheres spontaneously to microscope coverslips (37, 38). Cells were cultured at 30°C from frozen stocks to late logarithmic phase in tryptone broth that contained 100 μM arabinose and 50 μg ml$^{-1}$ ampicillin. Cells were harvested by centrifugation and suspended in motility medium (10 mM Tris, pH 7, 0.1 mM EDTA).

**Motility assay.** The rotation of single flagellar motors on tethered cells was measured as previously reported (32, 33). The hydrostatic pressure of the chamber was increased and decreased in increments of 20 MPa. The pressure was regulated to within ±1 MPa. The time the cells spent at high pressure was ~30 min. After the release of pressure, all cells were removed from the chamber, and the assay was repeated using cells that had not been exposed to high pressure. All assays were repeated with at least three different cultures. In addition, we confirmed that the applied pressure did not significantly change the physical characters, such as temperature, viscous drag, and pH, of the solution (20, 32).

## RESULTS

**Switching of motor rotation.** Figure 1a shows a schematic diagram of our high-pressure microscope (32). Hydrostatic pressure was applied to the pressure line using a hand pump. The pressure was applied to a buffer solution in a separator and then transmitted to the chamber. The internal pressure could be changed by several dozen MPa within a few seconds without any overshooting. The pressure device can be used for application of pressures up to 150 MPa, which is about 1.5 times higher than the water pressure at the deepest part of the Mariana Trench, the Challenger Deep (10,900 m). Thus, the device can be used to study most biological activities at various hydrostatic pressures on Earth. The experimental temperature was controlled by passing water from a temperature-regulated water bath through the chamber flow paths.

A single flagellar filament from bacteria that lack the switch-inducing protein CheY, because they have the *cheY* gene deleted, was tethered directly to the observation window of the high-pressure chamber. We observed spinning tethered cells to monitor the performance of single flagellar motors at various pressures and temperatures. All of the cells rotated exclusively in a CCW direction under ambient conditions (0.1 MPa and 20°C), as expected.

Figure 1b and c show sequential phase-contrast images of the same single cell at 0.1 and 120 MPa, respectively. The time courses of the rotation of the cell at various pressures are displayed in Fig. 1d. Below 40 MPa, the motor rotated smoothly in the CCW direction, and the rotational speed did not change significantly upon application of pressure. At 80 MPa, the rotational speed decreased sharply, but the motor still rotated in the CCW direction, as had been seen in our previous study (32, 33). At 120 MPa, the motor rotated still more slowly, but in the CW direction. Likewise, we found that many other cells still rotated in the CCW direction, changed direction frequently ("fluctuated"), or stopped rotation completely at 120 MPa (see Movie S1 and Fig. S1 in the supplemental material).

Next, we monitored the motility of motors at a pressure of 60 MPa when the temperature was decreased in a stepwise manner from 23 to 9°C. Figure 1e summarizes the time courses of the rotations of the same cell at various temperatures. At 15°C, the motor still rotated CCW, but it reversed to CW rotation at 9°C. The reversal in rotational direction occurred at a higher temperature than had been observed in a previous study in which flagellar motors rotated exclusively CW at −2°C when the hydrostatic pressure was 0.1 MPa (34). Thus, it suggests that increased pres-

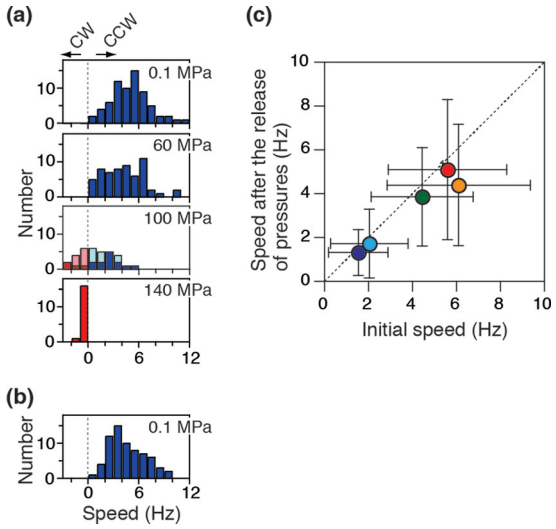


**FIG 2** Reversibility of rotation in tethered cells. (a and b) Histograms of the rotational speed at 23°C. The speeds of the motors rotating in the CCW and CW directions were taken as positive (blue) and negative (red), respectively. For motors in the fluctuation state, the speeds in CCW (pale blue) and CW (pale red) directions were analyzed separately (see Fig. S1 in the supplemental material) and plotted. Pressure was increased from 0.1 to 140 MPa in stages (a) and then decreased to 0.1 MPa (b). Data for the motors that were in the stop state were excluded from the histograms in panel a. (c) Reversibility of the rotational speed. The speed after the release of pressure was plotted against the initial speed at 0.1 MPa (mean ± SD; 5 [dark blue], 10 [light blue], 15 [green], 20 [orange], and 23°C [red]).

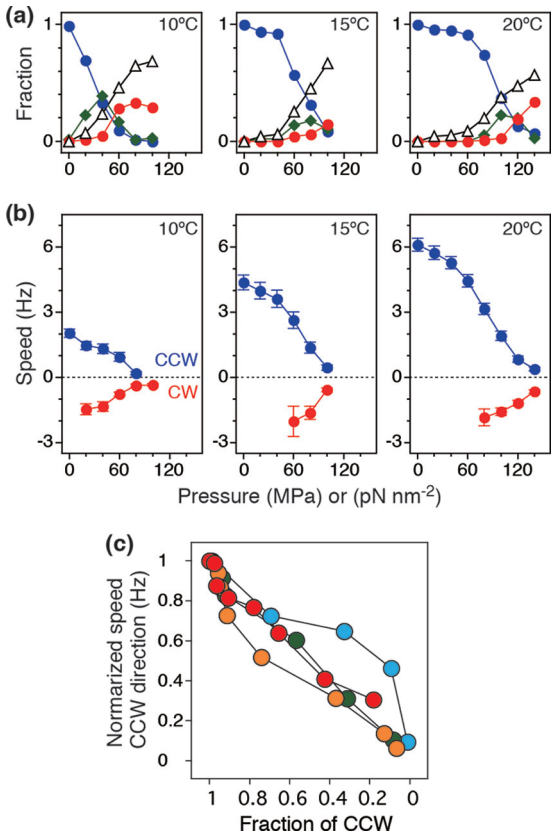


**FIG 3** Analysis of rotational direction and speed. (a) Fractions of cells in the CCW (blue), fluctuation (green), CW (red), and stop (white) states at 10, 15, and 20°C. (b) Pressure and speed relationships at 10, 15. and 20°C (mean ± standard error of the mean [SEM]). (c) Correlation between rotational direction and speed of motors at 10 (light blue), 15 (green), 20 (orange), and 23°C(red). The data at 5°C were removed from the analysis because the fraction of cells in the CCW state at 0.1 MPa was 0.72, which is already very different from 1.

sure and decreased temperature act in a complementary fashion to reverse motor rotation from CCW to CW. The details of the dependence on the pressure and temperature are discussed in more depth below.

**Reversibility of the effects of high pressure on motor rotation.** After application and release of pressure, we found that some tethered cells again began to rotate smoothly in the CCW direction. The motors on these cells showed that the pressure-induced switch in the direction of motor rotation can be reversible (see Movie S1 in the supplemental material). On the other hand, other cells did not recover to rotate CCW, possibly because they had become stuck to the observation window or because their motors had been irreversibly damaged in some way. The fraction of the motors showing the irreversible change depended on the temperature and the maximum pressure applied. To minimize these irreversible changes, we set the maximum pressures applied to 60 MPa at 5°C, 100 MPa at 10 and 15°C, and 140 MPa at 20 and 23°C. Under these conditions, half of the cells stopped rotating after the release of pressure. In the following analysis, we ignored cells that showed this irreversible change after application of high pressure.

Next, we checked the pressure dependence of changes in the rotational speed of cells that underwent reversible changes. The pressure was increased from 0.1 to 140 MPa in stages (Fig. 2a) and then decreased to 0.1 MPa (Fig. 2b). The fractions of cells showing fluctuation and stop states gradually increased with pressure. For cells whose direction of rotation fluctuated, the speeds in CCW (pale blue) and CW (pale red) directions were analyzed separately (see Fig. S1 in the supplemental material) and then plotted in Fig. 2a. Stopped cells were excluded from the histogram. The cells spun initially at 5.6 ± 2.7 Hz (mean ± standard deviation [SD]; $n = 84$) (Fig. 2a, top), and the speed decreased with pressure for most cells irrespective of rotational direction. After the release of pressure, the motors recovered to almost the same speed of 5.1 ± 3.2 Hz (mean ± SD; $n = 84$) (Fig. 2b) and rotated exclusively CCW. Figure 2c summarizes the reversibility of changes in the rotational speed at 5 to 23°C, showing that the temperature did not substantially impact the reversibility.

**Rotational direction and speed.** To quantify the effects of pressure and temperature on the motor direction, we monitored the same cells during the pressurization processes (0.1 to 140 MPa) at 5°C, 10°C, 15°C, 20°C, and 23°C (56 to 118 cells; 427 total). The cell behavior was classified into CCW, fluctuation, CW, and stop states by eye, and then the fractions were calculated for each pressure and temperature condition (Fig. 3a). At 20°C, the fraction of cells in the CCW state was almost equal to 1 when the pressure was less than 60 MPa. At more than 80 MPa, the fraction of cells in the CCW state decreased and reached ~0.1 at 140 MPa. On the other hand, the fraction of cells in the fluctuation state increased with pressure. After reaching a peak at 100 MPa, the fraction decreased with pressure. The number of cells in the stop and CW states monotonically increased with pressure. At lower temperatures (10 and 15°C in Fig. 3a), switching from CCW to the other states occurred even at lower pressures.

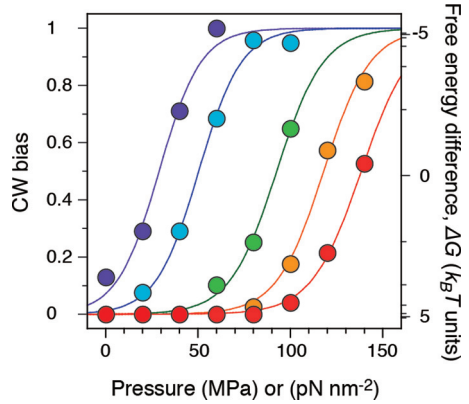


**FIG 4** CW bias. The experimental temperatures were 5 (dark blue), 10 (light blue), 15 (green), 20 (orange), and 23°C (red) (34 to 90 different motors were analyzed at each temperature). The plot at each temperature could be fitted by a sigmoidal curve (see the text).

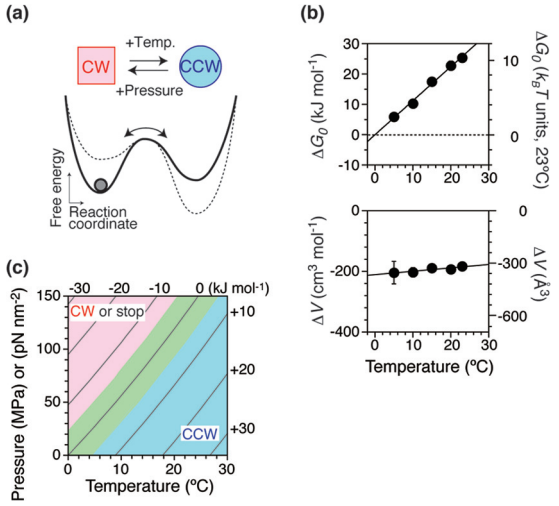


**FIG 5** Thermodynamics of switching in motor rotation. (a) Schematic free-energy diagram showing the equilibrium relation between CCW and CW states before (dashed line) and after (solid line) application of pressure. (b) Thermodynamic parameters. (Top) Free-energy difference at 0.1 MPa; $\Delta G_0$. The standard enthalpy and entropy were $-310$ kJ mol$^{-1}$ and $-1.1$ kJ $K^{-1}$ mol$^{-1}$, respectively. (Bottom) Pressure dependence parameter (reaction volume; $\Delta V$). The plots could be fitted by $\alpha \cdot (273 + T) + \beta$, where $\alpha$ is equal to 1.1 cm$^3$ mol$^{-1}$ $K^{-1}$ and $\beta$ is equal to $-510$ cm$^3$ mol$^{-1}$. (c) Pressure-temperature phase diagram. The value of $\Delta G$ is represented by gray curves at intervals of 10 kJ mol$^{-1}$. The blue, green, and red regions correspond to CW biases of $<0.1$, 0.1 to 0.9, and $>0.9$, respectively. The diagram was constructed using $\alpha$ and $\beta$, the standard enthalpy and entropy in panel b.

Next, we measured the rotational speed of the cells in CCW and CW states; data for the stop states were excluded from the calculation of the speed (Fig. 3b). Each plot was calculated from the histogram, as shown in Fig. 2a. The rotational speed gradually decreased with pressure regardless of the rotational direction. The pressure dependence of the speed was similar to that of the fraction of the cells in the CCW state. Finally, we checked the correlation between the speed and the fraction of the cells in the CCW state (Fig. 3c). The speed in the CCW direction was normalized by the initial value at 0.1 MPa and then plotted against the fraction of motors in the CCW direction (Fig. 3c). The plots show that the rotational speed in both the CCW and CW directions was highly correlated with the overall decrease in the fraction of CCW-rotating cells.

**CW bias.** We characterized the pressure-induced changes in the rotational direction by calculating the probability that a motor rotates in the CW direction (CW bias) and summarized the results in Fig. 4. The CW bias value at each pressure and temperature was calculated from the following equation: CW bias = $(n_{CW} + n_{fluctuation} \times f)/(n_{CW} + n_{fluctuation} + n_{CCW})$, where $n_{CW}$, $n_{fluctuation}$, and $n_{CCW}$ are the numbers of the motors in the CW, fluctuation, and CCW states, respectively; $f$ is the CW bias factor, or the probability that the motor in the fluctuation state rotates CW. The values of $f$ increased with pressure (see Fig. S1 in the supplemental material). Data for cells whose motors were stopped were excluded from calculation of the CW bias. The relationship between CW bias and applied pressure had similar sigmoidal curves, with the shift depending on temperature, indicating that the motor direction is sensitive to pressure. The CW bias value at 20°C (orange in Fig. 4) steeply increased with pressure and reached 0.5 at ~120 MPa. The pressure required to generate a CW bias of 0.5 increased linearly with temperature (see Fig. S2 in the supplemental material). In addition, the CW bias value was ~0.1 at 5°C and 0.1 MPa, which is quite consistent with previous studies (34).

In previous studies, such ultrasensitive switching has been explained by a two-state model in which the CCW and CW states are near equilibrium (Fig. 5a). Here, we have assumed that the free-energy potential profile can be changed by application of pressure. The equilibrium constant between the CCW and CW states, $K$, is defined as $\exp[-(\Delta G_0 + P\Delta V)/k_BT]$, where $\Delta G_0$ is standard free energy, $P$ is pressure, $\Delta V$ is a pressure-dependence parameter (reaction volume), $k_B$ is the Boltzmann constant, and $T$ is the experimental temperature. The CW bias can be described by $(1 + K^{-1})^{-1}$. Thus, the pressure and CW bias relation can be fitted by the following equation: CW bias = $(1 + \exp\{[\Delta G_0 + P\Delta V]/k_BT\})^{-1}$, where $\Delta G_0$ is equal to 9.4 $k_BT$ (equal to 23 kJ mol$^{-1}$) and $\Delta V$ is equal to $-320$ Å$^3$ (equal to $-190$ cm$^3$ mol$^{-1}$) at 20°C. Figure 5b summarizes the $\Delta G_0$ and $\Delta V$ values at 5 to 23°C. The upper graph shows that $\Delta G_0$ decreases linearly with decreased temperature and reaches zero at 0°C (indicated by the dotted line), a result consistent with previous work (34). On the other hand, $\Delta V$ is almost totally independent of temperature (lower graph). Figure 5c displays the pressure-temperature phase diagram of $\Delta G$, which was constructed from the thermodynamic parameters in Fig. 5b. The diagram shows that $\Delta G$ changes by 10 kJ mol$^{-1}$ for every ~40 MPa of pressure or ~8°C of temperature. The motor thus responds linearly to both pressure and temperature. Despite the complicated structure of the flagellar motor, which is composed of many copies of a number of different proteins, motor rotation can be described by simple thermodynamics.

## DISCUSSION

In this study, we characterized the pressure and temperature dependence of the motility of single flagellar motors in *E. coli* cells. In general (39), the application of pressures up to ~100 MPa (100 pN nm$^{-2}$) does not seriously affect the primary and secondary structures of protein molecules, but it does enhance the clustering of water molecules on the protein surface. This hydrated water often works to weaken protein-protein and protein-ligand interactions in solutions. Thus, application of ~100 MPa of pressure can, in principle, be used to change the function of flagellar mo-

tors without the use of any force-inducing tags (40, 41). In addition, at very high pressures (>500 MPa), protein aggregation and loss of secondary structure can occur due to hydration. Protein unfolding becomes irreversible at pressures above 500 MPa, and aggregation occurs. Here, we applied pressure up to 140 MPa and analyzed only the motor showing reversible changes against pressures. Thus, the applied pressure could slightly change the degree of hydration of the motor but not seriously damage its components.

The flagellar motors in a strain lacking the switch-inducing signaling protein, CheY, rotate exclusively in the CCW direction under normal ambient conditions (23°C; 0.1 MPa pressure). Here, we found that application of high pressure could induce CW rotation of flagellar motors without binding of CheY-P. A conformational change in the switch complex of the rotor is a good candidate for explaining our results. The switch complex forms the C ring on the cytoplasmic side of the rotor (42, 43). The C ring contains about 34 subunits of a structure consisting of ~1 monomer of FliG, 1 monomer of FliM, and a tetramer of FliN (44). FliG is thought to be important both for motor switching and for torque generation through its interaction with stator complexes containing 2 dimers of MotA and a single dimer of MotB ($MotA_4$/$MotB_2$) (45, 46). Some point mutations or deletions of a few specific residues in FliG lock motor rotation in either the CCW or CW direction (47–49). Several switching models have recently been reported based on structural differences between a CW-locked FliG mutant protein and wild-type FliG (15, 43, 49, 50).

In response to the binding of CheY-P to FliM and FliN (51), conformational changes in FliM and/or FliN molecules may stabilize FliG in its CW state. The CW bias of the flagellar motor depends greatly on the intracellular concentration of CheY-P and exhibits a Hill coefficient of ~10 (11). This relationship is similar to the dependence of the CW bias on increased pressure, for which a plot of CW bias versus pressure gave sigmoidal curves at all temperatures (Fig. 4). Thus, the application of pressure may change the equilibrium between the CCW and CW states of the switch complex in a similar manner as does the binding of CheY-P.

We performed a thermodynamic analysis (Fig. 5b) that revealed that the standard enthalpy and entropy for the equilibrium were $-306$ kJ $mol^{-1}$ and $-1.12$ kJ $K^{-1}$ $mol^{-1}$, respectively, a result that is consistent with previous studies (34). These values are similar to representative values ($-200$ kJ $mol^{-1}$ and $-0.5$ kJ $K^{-1}$ $mol^{-1}$) for protein folding at standard temperature and pressure (23°C; 0.1 MPa) (34, 52). Thus, the application of pressure partially collapses either the individual subunits or the integrated FliG-FliM-FliN protein components of the switch complex.

If we assume that the decrease in entropy during the transition from CCW to CW rotation is derived from the distribution of the hydrophobic interactions (the magnitude of the hydrophobic effect is $-0.6$ J $K^{-1}$ $mol^{-1}$ per Å$^2$ of nonpolar surface exposed to water) (34, 52), we arrive at an estimate of 54 Å$^2$ nonpolar surface exposed per subunit during the transition from CCW to CW. This value seems to be small compared with the total hydrophobic area on the exposed surfaces and/or interfaces of the component proteins (44, 53). Therefore, hydration of only a limited part of the surface area of the switch complex can apparently induce a large and cooperative structural change that leads to a reversal of rotational direction. To reach a good understanding of the phenomenon reported here, a more detailed analysis using molecular dynamics simulation will be required.

## ACKNOWLEDGMENTS

We thank Q. Ma and F. Bai for fruitful discussions; J. Armitage for the gift of strain JHC36; M. D. Manson, H. C. Berg, J. Yuan, T. Shimizu, and M. Baker for critically reading the manuscript; and I. Kawagishi, Y. Harada, S. Kojima, S. Kumazaki, and Y. Suzuki for technical support and discussions.

This work was supported by Grants-in-Aid from the Ministry of Education, Culture, Sports, Science and Technology, Japan (M.N. and Y.S.).

All experiments were performed by M.N.; data analysis was done by M.N and Y.S.; cultivation of the strain was arranged by M.H, A.I., and M.T.; the high-pressure chamber was designed by Y.K. and M.N.; and the manuscript was written by M.N. and Y.S.

## REFERENCES

1. **Manson MD.** 1992. Bacterial motility and chemotaxis. Adv. Microb. Physiol. **33**:277–346.
2. **Blair DF.** 1995. How bacteria sense and swim. Annu. Rev. Microbiol. **49**:489–522.
3. **Namba K, Vonderviszt F.** 1997. Molecular architecture of bacterial flagellum. Q. Rev. Biophys. **30**:1–65.
4. **Berg HC.** 2004. *E. coli* in motion. Springer, New York, NY.
5. **Porter SL, Wadhams GH, Armitage JP.** 2011. Signal processing in complex chemotaxis pathways. Nat. Rev. Microbiol. **9**:153–165.
6. **Berg HC.** 2003. The rotary motor of bacterial flagella. Annu. Rev. Biochem. **72**:19–54.
7. **Kojima S, Blair DF.** 2004. The bacterial flagellar motor: structure and function of a complex molecular machine. Int. Rev. Cytol. **233**:93–134.
8. **Sowa Y, Berry RM.** 2008. Bacterial flagellar motor. Q. Rev. Biophys. **41**:103–132.
9. **Minamino T, Imada K, Namba K.** 2008. Molecular motors of the bacterial flagella. Curr. Opin. Struct. Biol. **18**:693–701.
10. **Terashima H, Kojima S, Homma M.** 2008. Flagellar motility in bacteria structure and function of flagellar motor. Int. Rev. Cell Mol. Biol. **270**:39–85.
11. **Cluzel P, Surette M, Leibler S.** 2000. An ultrasensitive bacterial motor revealed by monitoring signaling proteins in single cells. Science **287**: 1652–1655.
12. **Duke TA, Le Novere N, Bray D.** 2001. Conformational spread in a ring of proteins: a stochastic approach to allostery. J. Mol. Biol. **308**:541–553.
13. **Bai F, Branch RW, Nicolau DV, Jr, Pilizota T, Steel BC, Maini PK, Berry RM.** 2010. Conformational spread as a mechanism for cooperativity in the bacterial flagellar switch. Science **327**:685–689.
14. **Ma Q, Nicolau DV, Jr, Maini PK, Berry RM, Bai F.** 2012. Conformational spread in the flagellar motor switch: a model study. PLoS Comput. Biol. **8**:e1002523. doi:10.1371/journal.pcbi.1002523.
15. **Stock D, Namba K, Lee LK.** 2012. Nanorotors and self-assembling macromolecular machines: the torque ring of the bacterial flagellar motor. Curr. Opin. Biotechnol. **23**:545–554.
16. **Abe F.** 2007. Exploration of the effects of high hydrostatic pressure on microbial growth, physiology and survival: perspectives from piezophysiology. Biosci. Biotechnol. Biochem. **71**:2347–2357.
17. **Oger PM, Jebbar M.** 2010. The many ways of coping with pressure. Res. Microbiol. **161**:799–809.
18. **Salmon ED, Ellis GW.** 1975. A new miniature hydrostatic pressure chamber for microscopy. Strain-free optical glass windows facilitate phase-contrast and polarized-light microscopy of living cells. Optional fixture permits simultaneous control of pressure and temperature. J. Cell Biol. **65**:587–602.
19. **Inoue S, Fuseler J, Salmon ED, Ellis GW.** 1975. Functional organization of mitotic microtubules. Physical chemistry of the in vivo equilibrium system. Biophys. J. **15**:725–744.
20. **Nishiyama M, Kimura Y, Nishiyama Y, Terazima M.** 2009. Pressure-induced changes in the structure and function of the kinesin-microtubule complex. Biophys. J. **96**:1142–1150.
21. **Nishiyama M, Shimoda Y, Hasumi M, Kimura Y, Terazima M.** 2010. Microtubule depolymerization at high pressure. Ann. N. Y. Acad. Sci. **1189**:86–90.
22. **Vass H, Black SL, Herzig EM, Ward FB, Clegg PS, Allen RJ.** 2010. A

multipurpose modular system for high-resolution microscopy at high hydrostatic pressure. Rev. Sci. Instrum. **81**:053710. doi:10.1063/1.3427224.
23. **Landau JV.** 1967. Induction, transcription and translation in Escherichia coli: a hydrostatic pressure study. Biochim. Biophys. Acta **149**:506–512.
24. **Paul KL, Morita RY.** 1971. Effects of hydrostatic pressure and temperature on the uptake and respiration of amino acids by a facultatively psychrophilic marine bacterium. J. Bacteriol. **108**:835–843.
25. **Yayanos AA, Pollard EC.** 1969. A study of the effects of hydrostatic pressure on macromolecular synthesis in Escherichia coli. Biophys. J. **9**:1464–1482.
26. **Morita RY, Zobell CE.** 1956. Effect of hydrostatic pressure on the succinic dehydrogenase system in Escherichia coli. J. Bacteriol. **71**:668–672.
27. **Welch TJ, Farewell A, Neidhardt FC, Bartlett DH.** 1993. Stress response of *Escherichia coli* to elevated hydrostatic pressure. J. Bacteriol. **175**:7170–7177.
28. **Ishii A, Sato T, Wachi M, Nagai K, Kato C.** 2004. Effects of high hydrostatic pressure on bacterial cytoskeleton FtsZ polymers in vivo and in vitro. Microbiology **150**:1965–1972.
29. **Zobell CE, Cobet AB.** 1962. Growth, reproduction, and death rates of *Escherichia coli* at increased hydrostatic pressures. J. Bacteriol. **84**:1228–1236.
30. **Meganathan R, Marquis RE.** 1973. Loss of bacterial motility under pressure. Nature **246**:525–527.
31. **Eloe EA, Lauro FM, Vogel RF, Bartlett DH.** 2008. The deep-sea bacterium Photobacterium profundum SS9 utilizes separate flagellar systems for swimming and swarming under high-pressure conditions. Appl. Environ. Microbiol. **74**:6298–6305.
32. **Nishiyama M, Sowa Y.** 2012. Microscopic analysis of bacterial motility at high pressure. Biophys. J. **102**:1872–1880.
33. **Nishiyama M, Kojima S.** 2012. Bacterial motility measured by a miniature chamber for high-pressure microscopy. Int. J. Mol. Sci. **13**:9225–9239.
34. **Turner L, Caplan SR, Berg HC.** 1996. Temperature-induced switching of the bacterial flagellar motor. Biophys. J. **71**:2227–2233.
35. **Inoue Y, Lo CJ, Fukuoka H, Takahashi H, Sowa Y, Pilizota T, Wadhams GH, Homma M, Berry RM, Ishijima A.** 2008. Torque-speed relationships of Na+-driven chimeric flagellar motors in *Escherichia coli*. J. Mol. Biol. **376**:1251–1259.
36. **Blair DF, Berg HC.** 1988. Restoration of torque in defective flagellar motors. Science **242**:1678–1681.
37. **Kuwajima G.** 1988. Construction of a minimum-size functional flagellin of *Escherichia coli*. J. Bacteriol. **170**:3305–3309.
38. **Berg HC, Turner L.** 1993. Torque generated by the flagellar motor of *Escherichia coli*. Biophys. J. **65**:2201–2216.
39. **Boonyaratanakornkit BB, Park CB, Clark DS.** 2002. Pressure effects on intra- and intermolecular interactions within proteins. Biochim. Biophys. Acta **1595**:235–249.
40. **Berry RM, Berg HC.** 1997. Absence of a barrier to backwards rotation of the bacterial flagellar motor demonstrated with optical tweezers. Proc. Natl. Acad. Sci. U. S. A. **94**:14433–14437.
41. **Pilizota T, Bilyard T, Bai F, Futai M, Hosokawa H, Berry RM.** 2007. A programmable optical angle clamp for rotary molecular motors. Biophys. J. **93**:264–275.
42. **Suzuki H, Yonekura K, Namba K.** 2004. Structure of the rotor of the bacterial flagellar motor revealed by electron cryomicroscopy and single-particle image analysis. J. Mol. Biol. **337**:105–113.
43. **Lee LK, Ginsburg MA, Crovace C, Donohoe M, Stock D.** 2010. Structure of the torque ring of the flagellar motor and the molecular basis for rotational switching. Nature **466**:996–1000.
44. **Brown PN, Terrazas M, Paul K, Blair DF.** 2007. Mutational analysis of the flagellar protein FliG: sites of interaction with FliM and implications for organization of the switch complex. J. Bacteriol. **189**:305–312.
45. **Garza AG, Harris-Haller LW, Stoebner RA, Manson MD.** 1995. Motility protein interactions in the bacterial flagellar motor. Proc. Natl. Acad. Sci. U. S. A. **92**:1970–1974.
46. **Zhou J, Lloyd SA, Blair DF.** 1998. Electrostatic interactions between rotor and stator in the bacterial flagellar motor. Proc. Natl. Acad. Sci. U. S. A. **95**:6436–6441.
47. **Magariyama Y, Yamaguchi S, Aizawa S.** 1990. Genetic and behavioral analysis of flagellar switch mutants of Salmonella typhimurium. J. Bacteriol. **172**:4359–4369.
48. **Togashi F, Yamaguchi S, Kihara M, Aizawa SI, Macnab RM.** 1997. An extreme clockwise switch bias mutation in fliG of Salmonella typhimurium and its suppression by slow-motile mutations in motA and motB. J. Bacteriol. **179**:2994–3003.
49. **Minamino T, Imada K, Kinoshita M, Nakamura S, Morimoto YV, Namba K.** 2011. Structural insight into the rotational switching mechanism of the bacterial flagellar motor. PLoS Biol. **9**:e1000616. doi:10.1371/journal.pbio.1000616.
50. **Lam KH, Ip WS, Lam YW, Chan SO, Ling TK, Au SW.** 2012. Multiple conformations of the FliG C-terminal domain provide insight into flagellar motor switching. Structure **20**:315–325.
51. **Sarkar MK, Paul K, Blair D.** 2010. Chemotaxis signaling protein CheY binds to the rotor protein FliN to control the direction of flagellar rotation in *Escherichia coli*. Proc. Natl. Acad. Sci. U. S. A. **107**:9370–9375.
52. **Privalov PL.** 1992. Protein folding. W. H. Freeman and Co, New York, NY.
53. **Paul K, Harmon JG, Blair DF.** 2006. Mutational analysis of the flagellar rotor protein FliN: identification of surfaces important for flagellar assembly and switching. J. Bacteriol. **188**:5240–5248.